Efficient free-space read-out of WGM lasers using circular micromirrors

Tobias Wienhold,[1,*] Sarah Kraemmer,[2] Andreas Bacher,[1] Heinz Kalt,[2] Christian Koos,[1,3] Sebastian Koeber,[1,3] and Timo Mappes[1,4]

[1]*Institute of Microstructure Technology, Karlsruhe Institute of Technology, 76128 Karlsruhe, Germany*
[2]*Institute of Applied Physics, Karlsruhe Institute of Technology, 76128 Karlsruhe, Germany*
[3]*Institute of Photonics and Quantum Electronics, Karlsruhe Institute of Technology, 76128 Karlsruhe, Germany*
[4]*Now with Carl Zeiss AG, Corporate Research and Technology, 07745, Jena, Germany*
[*]*tobias.wienhold@kit.edu*

Abstract: Lasing from whispering-gallery mode (WGM) resonators occurs omnidirectional in azimuthal plane. Most applications of WGM resonators require spectral analysis with off-chip detectors, where in-plane emission and beam divergence hinder efficient detection. We demonstrate redirecting WGM laser emission from all azimuthal angles using a circular micromirror placed around the cavity. By collecting reflections off the micromirror via free-space optics, read-out intensity improved by one order of magnitude. Blocking vertically emitted spontaneous emission and recording reflections off the micromirror only, signal-to-noise ratio improved from 4.6 dB to 15 dB. Our read-out concept may be applied to arbitrary WGM cavity geometries without deteriorating the cavity's quality factor.

OCIS codes: (140.3945) Microcavities; (140.2050) Dye lasers; (160.5470) Polymers; (220.4000) Microstructure fabrication.

References and links

1. S. Mehrabani, P. Kwong, M. Gupta, and A. M. Armani, "Hybrid microcavity humidity sensor," Appl. Phys. Lett. **102**(24), 241101 (2013).
2. A. Harker, S. Mehrabani, and A. M. Armani, "Ultraviolet light detection using an optical microcavity," Opt. Lett. **38**(17), 3422–3425 (2013).
3. E. J. Smith, S. Schulze, S. Kiravittaya, Y. Mei, S. Sanchez, and O. G. Schmidt, "Lab-in-a-tube: detection of individual mouse cells for analysis in flexible split-wall microtube resonator sensors," Nano Lett. **11**(10), 4037–4042 (2011).
4. J. Zhu, S. K. Ozdemir, Y.-F. Xiao, L. Li, L. He, D.-R. Chen, and L. Yang, "On-chip single nanoparticle detection and sizing by mode splitting in an ultrahigh-Q microresonator," Nat. Photonics **4**(1), 46–49 (2010).
5. F. Vollmer and S. Arnold, "Whispering-gallery-mode biosensing: label-free detection down to single molecules," Nat. Methods **5**(7), 591–596 (2008).
6. F. Vollmer, S. Arnold, and D. Keng, "Single virus detection from the reactive shift of a whispering-gallery mode," Proc. Natl. Acad. Sci. U.S.A. **105**(52), 20701–20704 (2008).
7. J. C. Knight, G. Cheung, F. Jacques, and T. A. Birks, "Phase-matched excitation of whispering-gallery-mode resonances by a fiber taper," Opt. Lett. **22**(15), 1129–1131 (1997).
8. M. Cai, O. Painter, and K. J. Vahala, "Observation of Critical Coupling in a Fiber Taper to a Silica-Microsphere Whispering-Gallery Mode System," Phys. Rev. Lett. **85**(1), 74–77 (2000).
9. M. Fujiwara, K. Toubaru, and S. Takeuchi, "Optical transmittance degradation in tapered fibers," Opt. Express **19**(9), 8596–8601 (2011).
10. J. Van Campenhout, P. Rojo Romeo, P. Regreny, C. Seassal, D. Van Thourhout, S. Verstuyft, L. Di Cioccio, J.-M. Fedeli, C. Lagahe, and R. Baets, "Electrically pumped InP-based microdisk lasers integrated with a nanophotonic silicon-on-insulator waveguide circuit," Opt. Express **15**(11), 6744–6749 (2007).
11. A. Tulek, D. Akbulut, and M. Bayindir, "Ultralow threshold laser action from toroidal polymer microcavity," Appl. Phys. Lett. **94**(20), 203302 (2009).
12. A. Schawlow and C. Townes, "Infrared and Optical Masers," Phys. Rev. **112**(6), 1940–1949 (1958).
13. T. Grossmann, S. Schleede, M. Hauser, M. B. Christiansen, C. Vannahme, C. Eschenbaum, S. Klinkhammer, T. Beck, J. Fuchs, G. U. Nienhaus, U. Lemmer, A. Kristensen, T. Mappes, and H. Kalt, "Low-threshold conical microcavity dye lasers," Appl. Phys. Lett. **97**(6), 063304 (2010).
14. T. Grossmann, S. Schleede, M. Hauser, T. Beck, M. Thiel, G. von Freymann, T. Mappes, and H. Kalt, "Direct laser writing for active and passive high-Q polymer microdisks on silicon," Opt. Express **19**(12), 11451–11456 (2011).

#225019 - $15.00 USD Received 16 Oct 2014; revised 6 Dec 2014; accepted 8 Dec 2014; published 16 Jan 2015

15. J. Wiersig and M. Hentschel, "Unidirectional light emission from high-Q modes in optical microcavities," Phys. Rev. A **73**(3), 031802 (2006).
16. Q. J. Wang, C. Yan, N. Yu, J. Unterhinninghofen, J. Wiersig, C. Pflügl, L. Diehl, T. Edamura, M. Yamanishi, H. Kan, and F. Capasso, "Whispering-gallery mode resonators for highly unidirectional laser action," Proc. Natl. Acad. Sci. U.S.A. **107**(52), 22407–22412 (2010).
17. G. D. Chern, H. E. Tureci, A. D. Stone, R. K. Chang, M. Kneissl, and N. M. Johnson, "Unidirectional lasing from InGaN multiple-quantum-well spiral-shaped micropillars," Appl. Phys. Lett. **83**(9), 1710 (2003).
18. X.-F. Jiang, Y.-F. Xiao, C.-L. Zou, L. He, C.-H. Dong, B.-B. Li, Y. Li, F.-W. Sun, L. Yang, and Q. Gong, "Highly unidirectional emission and ultralow-threshold lasing from on-chip ultrahigh-Q microcavities," Adv. Mater. **24**, OP260–4, OP185 (2012).
19. J. Pomplun, S. Burger, L. Zschiedrich, and F. Schmidt, "Adaptive finite element method for simulation of optical nano structures," Phys. Status Solidi **244**(10), 3419–3434 (2007).
20. T. Grossmann, M. Hauser, T. Beck, C. Gohn-Kreuz, M. Karl, H. Kalt, C. Vannahme, and T. Mappes, "High-Q conical polymeric microcavities," Appl. Phys. Lett. **96**(1), 013303 (2010).
21. T. Grossmann, T. Wienhold, U. Bog, T. Beck, C. Friedmann, H. Kalt, and T. Mappes, "Polymeric photonic molecule super-mode lasers on silicon," Light Sci. Appl. **2**(5), e82 (2013).

1. Introduction

Whispering-gallery mode (WGM) resonators have been demonstrated as highly sensitive detectors for humidity [1], UV light [2], single cells [3], or nanoparticles [4]. Especially the field of biosensing has been investigated in detail during the past years [5]. Sensing applications utilize the interaction of the evanescent part of the cavity modes with the surrounding media, i.e. the analyte. High quality factors achieved with microshpere and microtoroid resonators have enabled detection of low particle concentrations down to single viruses [6]. Due to the small cavity sizes, the scalability of their fabrication via established semiconductor processes, their high sensitivity, and versatile usability, WGM resonators have been proposed for compact, portable, and low-cost sensor platforms, so called Lab-on-a-Chip (LoC) systems. However, only few WGM sensor concepts have actually been utilized outside of a very defined and controlled lab surrounding. One significant restriction that limits integration into LoCs is excitation and read-out of WGM resonators, which is commonly done via evanescent field coupling. Here, the evanescent part of guided modes, e.g., in an adiabatically tapered fiber, is used to excite the WGMs in the cavity [7,8]. While evanescent coupling allows efficient excitation of WGMs and read-out of spectral shifts, taper fabrication and handling is not applicable outside a controlled laboratory environment due to elaborate fabrication and taper fragility. Additionally, alignment of resonator and fiber taper with nanometer precision is required to enable coupling, and taper lifetime is limited [9].

Evanescent coupling can be overcome by integrating a gain medium into the WGM cavity, thereby transforming the passive resonator to a microcavity laser that can be pumped electrically [10] or optically with an external light source [11]. An additional advantage of laser cavities in comparison to passive cavities is reduced emission linewidth [12]. Dye molecules have been demonstrated as particularly efficient gain media in polymeric cavities enabling efficient pumping of the WGMs via free-space optics [13,14]. Collection of the WGM laser emission can also be achieved via free-space optics positioned on top or at the side of the resonators. However, efficiency of both techniques is limited by collecting solely a small fraction of the emitted radiation. This is undesired since tracking of the resonance peaks requires distinct lasing peaks with high signal-to-noise ratio. To direct more light onto the detector, directed emission from WGM resonators is required. Several approaches have been reported realizing directional emission by modifying the cavity shape with notches [15,16], spirals [17], or ellipses supporting so called "chaotic modes" [18]. These approaches allow highly directed in-plane emission, but often reduce the cavity's quality factor and are limited to certain material systems and cavity geometries.

In this paper we present and experimentally demonstrate a novel read-out concept for WGM laser emission that relies on redirecting the cavity's emission with a circular micromirror positioned around the cavity. Our finite element simulations show that emission from microgoblet resonators due to radiation loss is confined to the horizontal direction. For a surface of the mirror angled at 45°, the horizontally emitted laser light is reflected vertical to the substrate. Circularity of the micromirror allows redirection of the laser emission from all

#225019 - $15.00 USD Received 16 Oct 2014; revised 6 Dec 2014; accepted 8 Dec 2014; published 16 Jan 2015

azimuthal angles, enabling efficient collection with an off-chip detector. This approach is applicable to arbitrary cavity geometries and does not reduce the cavity's quality factor.

2. Finite element method (FEM) simulations of microgoblet resonators

Emission from WGM lasers may be considered as cavity loss. Loss mechanisms contributing to emission from WGMs include scattering from contaminants or surface defects along the resonator circumference and radiation loss of the WGMs due to curvature of the cavity outline. Scattering centers may be assumed randomly distributed and emission from these sites occurs with no inherent directionality. Radiation loss of WGMs is strongly dependent on the cavity geometry. In order to analyze the emission profile from microgoblet resonators, FEM simulations with the JCMsuite software (JCMwave GmbH) were performed. Figure 1(a) shows the modeled cavity, materials, and the computational domain used for the simulations. The cavity dimensions and shape were modeled according to scanning electron micrographs of fabricated microgoblet lasers. Perfectly matched layers (PML) were used in order to realize transparent boundary conditions. To reduce computational costs the rotational symmetry of the device was utilized and only one radial section of microgoblet resonator was used for the simulation. Detailed information about the utilized algorithm has been published by Pomplun et al. [19]. A detailed investigation of the mode patterns in WGM microgoblet resonators has been reported by Grossmann et al. [20]. For our case the eigenfrequencies and respective electric field distributions of a passive microgoblet resonator were computed for an azimuthal mode number of m = 303, specifying the integer number of wavelengths along one cavity round trip. The simulated electric field distribution of the fundamental transversal electric (TE) mode is depicted in Fig. 1(d) for a wavelength of 623.8 nm. To visualize the directionality of radiation loss, the field amplitude was plotted on a logarithmic color scale. Additionally, the field amplitude profiles along the top and the left side of the simulation field were plotted at equal distances from the mode field maximum and are depicted in Fig. 1(b) and Fig. 1(c), respectively. It is noted that in the area of Fig. 1(b), where no field amplitude is plotted, local field amplitude is below the lower limit of the axis. The ratio of the field amplitudes emitted vertical and horizontal to the mode maximum (positions indicated by grey dotted lines) exceeds ten orders of magnitude, verifying that radiation loss from the microgoblet cavity mainly occurs in horizontal direction. From the plotted amplitude profile in Fig. 1(c) a $1/e^2$ opening angle of the cavity emission due to radiation loss of 45.2° was determined.

#225019 - $15.00 USD Received 16 Oct 2014; revised 6 Dec 2014; accepted 8 Dec 2014; published 16 Jan 2015

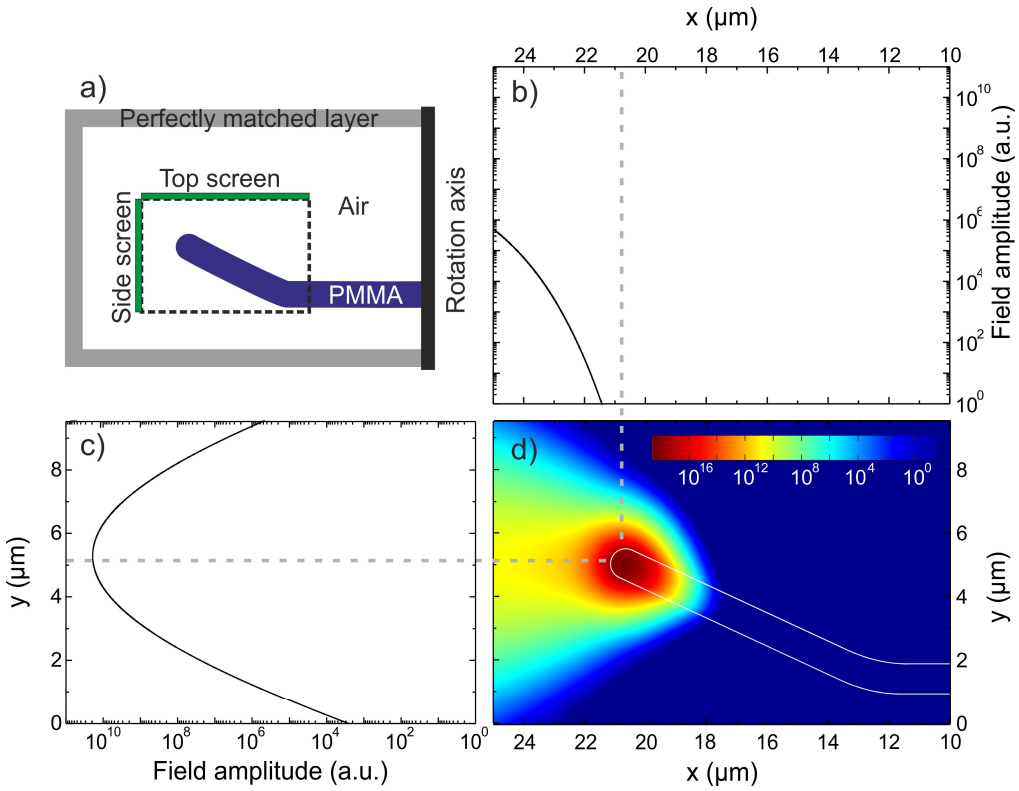

Fig. 1. FEM simulation of the electric field distribution (TE mode) of a microgoblet resonator: (a) Computational domain including the cross section of the modeled cavity, materials and screens. A perfectly matched layer surrounding the cavity is used to enable transparent boundary conditions. (d) Simulated electric field distribution of the fundamental TE mode at 623.8 nm. The plotted area is highlighted in (a) by the dotted rectangle. (b) and (c) show the intensity distribution along the screens positioned on top and the left side of (d), respectively. The grey dotted lines highlight the vertical and horizontal position of the field maximum of the WGM. It is noted that all field amplitudes are plotted on a logarithmic scale.

3. Concept of micromirror read-out

As emission occurs omnidirectional in azimuthal plane, efficient collection of laser emission from WGM resonators requires detecting radiation from all angles. Our proposed read-out concept is based on a circular micromirror placed around the cavity. Emission from the cavity is reflected off the micromirror surface vertical to the substrate. This read-out concept is depicted in Fig. 2. Light from a pump laser is focused loosely onto the cavity through a microscope objective to excite lasing in the cavity. Omnidirectional emission from the cavity is radiated mainly horizontally. The microgoblet laser is surrounded by a concentric micromirror with a reflecting surface angled at 45°. Emission into all azimuthal directions is reflected from the mirror surface vertical to the substrate. After reflection, light from all azimuthal directions is confined to a beam propagating in vertical direction and can be efficiently collected with an objective.

#225019 - $15.00 USD Received 16 Oct 2014; revised 6 Dec 2014; accepted 8 Dec 2014; published 16 Jan 2015

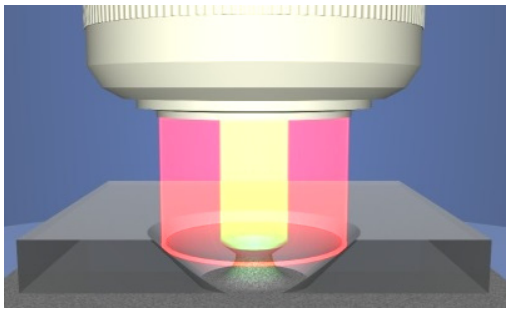

Fig. 2. Schematic of the micromirror read-out concept: The microgoblet laser is pumped through an objective from the top (yellow). Emission occurs omnidirectional in azimuthal direction but is confined in vertical direction. Emission from all azimuthal angles is reflected from the angled mirror surface vertical to the substrate and is collected with the objective (red).

4. Micromirror and microgoblet fabrication

For an experimental demonstration of the read-out concept, micromirrors and microgoblet lasers were fabricated on separate substrates and subsequently joined and bonded. Micromirrors with a reflecting surface angled at 45° were embossed into polymer foils by thermal nanoimprinting using a microstructured mold. Embossing parameters were optimized to achieve smooth mirror surfaces surrounding a concentric hole through the entire foils. To improve the mirror reflectivity, the angled surfaces were coated with aluminum. Structuring of the microgoblet lasers from poly (methyl methactylate) (PMMA) was done according to the previously published method involving electron beam lithography, selective undercutting with xenon difluoride (XeF_2), and a subsequent thermal reflow step [20]. The cavity of such resonators is elevated on a silicon pedestal raising the light-guiding cavity rim typically about 15 µm above the substrate surface. Replicated micromirrors showed increased surface roughness this close to the central hole. In order to have the emitted light incident on the middle part of the micromirror, where fabrication-induced defects on the reflective surface of the micromirror are lowest, microgoblets were raised onto double pedestals. To this end, two aligned exposures followed by xenon difluoride etching were performed, raising the resonator rim to about 80 µm above the substrate surface. In a final step, the microgoblets were aligned to the mirrors, threaded into the hole in the micromirrors, and both substrates were agglutinated using UV-curable adhesive.

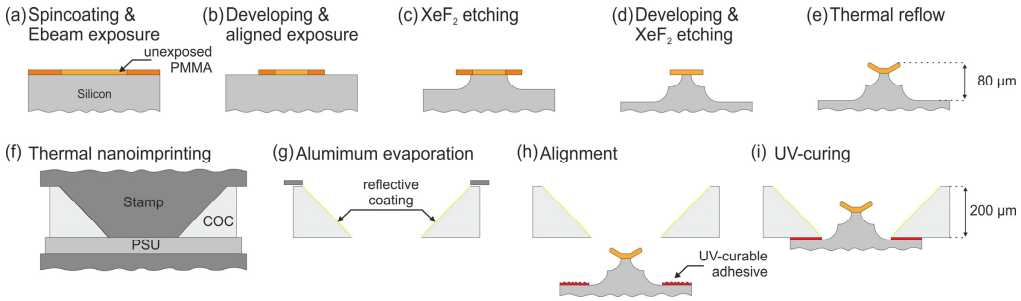

Fig. 3. Sketch of fabrication process: PMMA microgoblet lasers were fabricated via spin coating, electron beam exposure, isotropic etching with XeF_2, and subsequent thermal reflow. Micromirrors were imprinted into COC foils and angled surfaces were coated with aluminum through a shadow mask. After alignment, both substrates were agglutinated using UV-curable adhesive.

The detailed fabrication process of microgoblet resonators and micromirrors is depicted in Fig. 3. A microstructured metal mold with pins inversely shaped to the micromirrors was fabricated by precision turning. Pins were designed as flat top cones with a top diameter and height of 200 µm. The pins angle was designed to replicate mirrors with 45° reflecting

#225019 - $15.00 USD Received 16 Oct 2014; revised 6 Dec 2014; accepted 8 Dec 2014; published 16 Jan 2015

surfaces. A perfluorodecyltrichlorosilane (FDTS) anti-stick coating was deposited onto the mold via molecular vapor deposition to reduce the adhesion of the polymer to its surface. Subsequently, the mold was replicated into TOPAS COC 6013 (Topas Advanced Polymers) foils of 254 µm thickness by thermal nanoimprinting with a hot embossing machine (Jenoptik HEX 03). To produce holes that go through the COC foil with a smooth outline and to protect the mold's pins, a second polymer sheet was placed on the counter plate of the hot embossing machine as a buffer. Polysulfone (PSU) foils were chosen due to the higher glass transition temperature compared to COC. An imprinting temperature of 193°C and a pressure of 12.5 N/mm^2 were used for replication. As COC is highly transparent in the visible range, reflectivity of the angled surfaces was achieved by coating with a 60 nm thick aluminum layer via thermal evaporation. A shadow mask with openings above the micromirrors was used during evaporation to solely coat the angled surfaces and leave all other parts of the chip surrounding the mirrors uncoated.

Microgoblet lasers were fabricated from PMMA photoresist (MicroChem Corp.) dissolved in anisole. The dye pyrromethene 597 (Radiant Dyes Laser & Accessoires GmbH) was admixed to the solution at a concentration of 2.56×10^{-5} mol/g PMMA. The resist mixture was spin coated onto n-type silicon wafers at a thickness of 1.2 µm. Subsequently, PMMA was exposed with an electron beam (Vistec Electron Beam GmbH, VB6) to fabricate microdisks elevated on double pedestals. Firstly, PMMA was exposed and developed to form disks of 200 µm diameter. Afterwards an aligned electron beam lithography exposure was performed, leaving disks of 50 µm diameter in the center of the 200 µm diameter disks unexposed. Accurate concentricity of both exposures was achieved by alignment markers, which were etched into the silicon wafer before spin coating the PMMA. Following the second exposure, no immediate development was performed, leaving the 200 µm diameter PMMA disks as etching masks for pedestals. The PMMA disks were undercut symmetrically due to the isotropic etching performance of XeF_2. Etching was stopped at an undercut of about 65-70 µm. The previously exposed but undeveloped ring between the 50 and 200 µm diameter disks was now removed in a second developing step. The subsequent fabrication steps follow the previously published microgoblet fabrication process [20]. XeF_2 etching was used to undercut the rim of the PMMA disk, supporting the disk on a center pedestal. In a final thermal reflow step resonators were heated to 135°C on a hot plate in order to anneal defects along the outline of the PMMA disk utilizing softening of the polymer above its glass transition temperature. Figure 4 shows a scanning electron micrograph of a microgoblet resonator on a double pedestal.

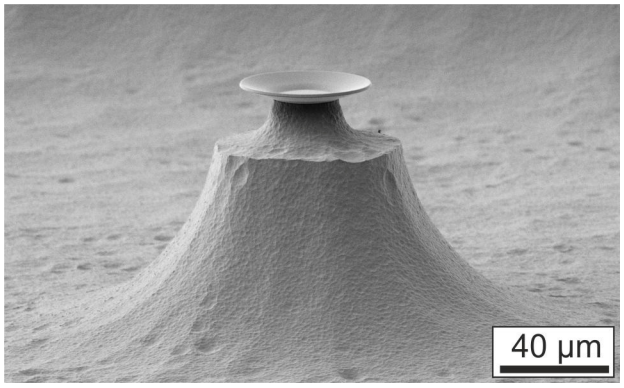

Fig. 4. SEM of microgoblet laser on double pedestal. The light-guiding rim of the resonator is elevated about 80 µm above the substrate surface using two aligned electron beam exposures followed by selective etching with XeF_2.

To assemble microgoblets and micromirrors, both substrates were placed parallel to each other leaving a spacing of few hundred micrometers. Substrates were aligned with micrometer stages with respect to lateral position and angle. Positioning was verified online using an

#225019 - $15.00 USD Received 16 Oct 2014; revised 6 Dec 2014; accepted 8 Dec 2014; published 16 Jan 2015

optical microscope. After successful alignment, the spacing between the substrates was reduced until the resonators protruded through the holes in the micromirrors' center. By placing the resonators on elevated pedestals, the light-guiding resonator rim was now located at the same height as the middle part of the reflection surface. UV curable adhesive was used to bond both substrates. Due to its solvent-free composition, low curing dose, and high chemical resistance, the photoresist Ormocomp was used as adhesive. As aluminum was deposited through a shadow mask, the top of the COC device was left uncoated to allow curing the adhesive through the transparent foil.

5. Optical characterization and measurement results

The optical performance of microgoblet lasers integrated with micromirrors was characterized by measuring lasing spectra, lasing thresholds, and spatially resolved emission patterns. The effect of the micromirror was evaluated by comparing the emission of the same sample with and without micromirrors. Figure 5(a) shows the setup used for optical characterization. Microgoblets were pumped with a frequency-doubled Nd:YLF crystal laser emitting nanosecond pulses at a wavelength of 523 nm, close to the absorption maximum of the dye. We used a pulse repetition rate of 20 Hz for all measurements. The pump pulse energy was adjusted by a rotating half-wave plate polarization controller followed by a polarization sensitive beam splitter. The pump beam was loosely focused onto the microgoblet through a microscope objective with 10x magnification and a numerical aperture of 0.2, providing a field of view that covers the full micromirror and still has a convenient working distance. Emission from the microgoblet reflected off the micromirror and was collected by the same objective. The emission was filtered from the pump beam by a dichroic filter and directed onto a CCD camera for imaging and a Czerny-Turner spectrometer (Shamrock 500i equipped with 1200 l/mm grating and Andor iDus 420 camera) for spectral analysis. A magnified intermediate image was created in the optical path and a variable aperture iris diaphragm was placed in position of the image plane. If the aperture was fully opened, light from resonator and micromirror was recorded by the CCD and the spectrograph. Closing the aperture diameter blanked light reflected off the micromirror and only allowed vertically emitted light from the central resonator to be recorded by the system. Additionally, a removable pin could be placed in the center of the iris diaphragm, blocking the emission from the resonator to record light reflected from the micromirror only. The inset in Fig. 5(b) shows a detailed sketch of this imaging control.

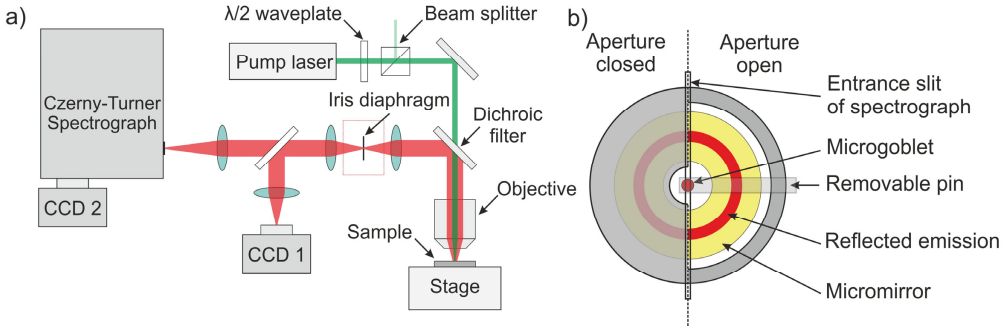

Fig. 5. (a) Microresonator characterization setup, (b) Spatial control of imaged field of view via iris diaphragm (positioned inside of red box in (a)). Right (Aperture fully open): Light from microgoblet and micromirror enters the spectrometer entrance slit. A removable pin can be inserted to block emission from the microgoblet. Left (Aperture closed): Only light from microgoblet can enter spectrometer.

Figure 6(a) shows the recorded input-output curve of a microgoblet laser integrated by a micromirror. A lasing threshold of 1.5 nJ per pulse was measured for the microgoblet laser on a double pedestal. To validate reflection of the emitted light off the micromirror, spatially resolved spectra were recorded with the spectrometer's entrance slit centered across the

#225019 - $15.00 USD Received 16 Oct 2014; revised 6 Dec 2014; accepted 8 Dec 2014; published 16 Jan 2015

micromirror. The spectrum in Fig. 6(b) shows four distinct horizontal lines (highlighted in red boxes) across the imaged area with intensity peaks at the lasing wavelengths. The inner two lines represent emission from the rims of the microgoblet resonator and the outer lines represent the reflections off the micromirror surface. On the inner spectra, a significant intensity can be seen over the whole spectral range, which can be attributed to the dye fluorescence. The spectra recorded from the upper and lower reflections off the micromirror show the lasing peaks with a significantly reduced fluorescence background. As fluorescence is emitted omnidirectional from the whole resonator volume, a significant amount is emitted upward directly into the objective. Due to the distance to the micromirror, fluorescence intensity after reflection off the mirror is significantly reduced due to divergence.

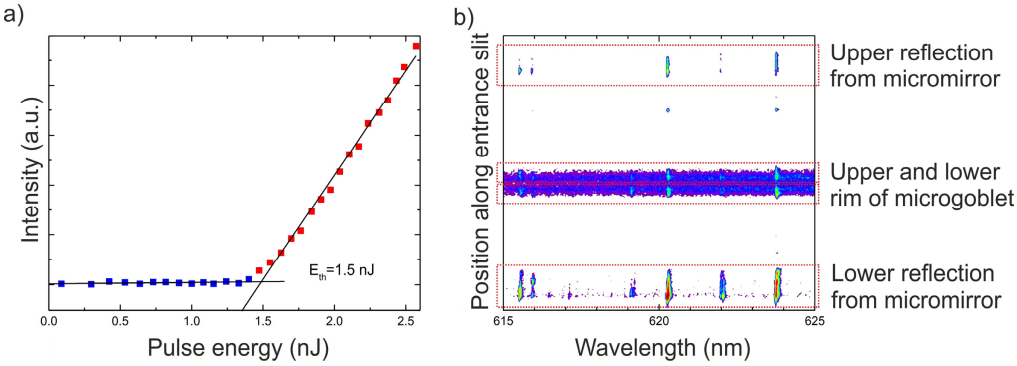

Fig. 6. (a) Microgoblet laser threshold curve at 623.78 nm with threshold energy E_{th} = 1.5 nJ. Data points below and above threshold are marked in blue and red, respectively. (b) Plot of spatially resolved spectrum along the spectrometer entrance slit. Reflection of lasing emission off the upper and lower mirror surface can be a seen as localized spectral peaks.

To characterize the influence of the micromirror on the detection efficiency, emission spectra of the resonators with and without the micromirror were recorded. The combined spectrum from microgoblet and micromirror was taken at fully opened aperture. To record the emission of the microgoblet laser only, the aperture of the iris diaphragm was closed to completely block emission from micromirror. In a third measurement, the aperture was left fully opened but a pin was moved into the center of the diaphragm, blocking the emission of the resonator and allowing only light reflected off the micromirror to be recorded. For all measurements the pump pulse energy was set to 2.6 nJ, significantly above threshold. Intensities were recorded without spatial resolution by integrating over the full CCD column for each wavelength (vertical binning mode). Figure 7 shows a plot of three recorded spectra for comparison of the detected intensities. Recording emission from the microgoblet only, lasing peaks were superimposed with a strong fluorescence signal. By collecting the emission from resonator and micromirror simultaneously, the lasing intensity was improved by a factor of up to 9.7 (λ = 623.78 nm). We attribute this increase of intensity using the micromirror to horizontal confinement of laser emission from WGM cavities. While only a fraction of the laser emission, which is scattered out of the horizontal plane, can be recorded straight from the top, reflecting the emission off the angled micromirror into off-chip direction increases the detectable intensity.

In contrast to stimulated emission, fluorescence is emitted omnidirectionally. While the recorded lasing peak intensity increased by a factor of 9.7 using the micromirror, fluorescence intensity only increased by a factor of 1.5. This resulted in an increase of the signal-to-noise ratio (SNR) from 4.6 dB when recording only the resonator, to 11.3 dB detecting resonator and micromirror simultaneously. The SNR was calculated as the ratio of maximum peak intensity to average fluorescence background close to the peak. To further increase the SNR, the upward emission from the microgoblet was blocked with a pin in the image plane. In comparison to recording emission from resonator and micromirror simultaneously, the

#225019 - $15.00 USD Received 16 Oct 2014; revised 6 Dec 2014; accepted 8 Dec 2014; published 16 Jan 2015

detected fluorescence intensity was reduced by a factor of 3, while the peak intensity was only reduced by a factor of 1.25, yielding a maximum SNR of 15 dB (λ = 623.78 nm).

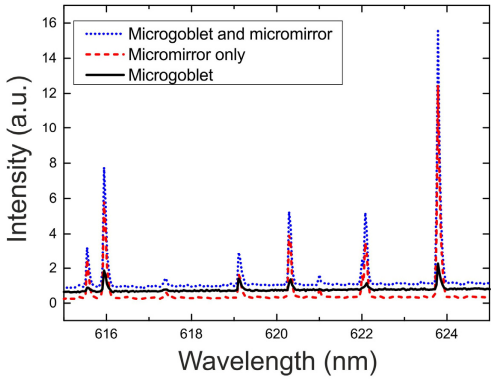

Fig. 7. Comparison of lasing spectra recorded with (blue) and without the micromirror (black): By detecting emission from microgoblet and micromirror simultaneously, the laser intensity can be increased by up to 9.7 compared to read-out without a mirror. Blocking the direct emission from the microgoblet and recording the reflections from the micromirror only (red), yields an increase in SNR of up to 15 dB (both measured at λ = 623.78 nm).

6. Comparison of simulation data and measurement results

From the FEM simulations an opening angle of 45.2° in horizontal plane was calculated for emission from the microgoblet cavity. For the ease of use of the microgoblet resonators in a future sensing scheme, a microscope objective with a long working distance is required in the setup. A long working distance however results in a low numerical aperture. The microscope objective used for optical pumping and optical characterization has a working distance of 13 mm, and a numerical aperture of 0.2. Therefore, it is expected that emission in horizontal plane cannot efficiently be collect with the objective. Our experiments validate this assumption, as a 9.7 time increase in the recorded laser intensity was achieved by additionally collecting reflections from the micromirror. With a radial distance of the microgoblet rim to the reflective surface of the micromirror of about 160 µm, the beam should expand to a $1/e^2$ height of 130 µm on the reflective surface. This approximation is in good agreement with the broad intensity distribution recorded across the micromirror (see Fig. 6(b)). The intensity of the laser peaks recorded with a closed aperture may be attributed to scattering loss from the WGMs due to contaminants or surface defects along the resonator circumference.

7. Conclusion

We have demonstrated enhanced read-out efficiency of WGM lasers using circular micromirrors placed around the cavity. Lasing from WGMs, which is emitted omnidirectional in azimuthal plane, reflects off the angled micromirror surface and is collected via free-space optics. To our best knowledge this concept is the first realization of vertically redirected WGM emission. We have performed FEM simulations to obtain the emission patterns of microgoblet resonators in vertical and horizontal direction. The micromirror read-out concept has been theoretically supported by the fact that emission due to radiation loss predominantly occurs in horizontal direction. Microgoblet lasers made from PMMA admixed with a laser dye were structured by electron beam lithography and subsequent underetching with XeF_2. Micromirrors fabricated from COC foils by thermal nanoimprinting were coated with aluminum to increase the reflectivity. To optimize read-out efficiency, microgoblets were elevated on double pedestals, raising the resonator rim 80 µm above the substrate surface to the middle part of the micromirror. We validated the read-out concept by spatially resolved spectra, showing localized spectral peaks on the mirror surface. An increase in laser peak intensity by 9.7 was demonstrated while fluorescence intensity increased merely 1.5 times. To

#225019 - $15.00 USD Received 16 Oct 2014; revised 6 Dec 2014; accepted 8 Dec 2014; published 16 Jan 2015

maximize the signal-to-noise ratio (laser peak intensity to fluorescence background), we blocked spontaneous emission vertical to the substrate. A maximum signal-to-noise ratio of 15 dB was achieved, when recording reflections off the micromirror only. The recorded spatially resolved spectra are in good agreement with the emission profiles determined by our simulations.

Previous approaches realized directed azimuthal emission by altering the cavity outline. Our concept of redirecting the emission vertically with a micromirror is particularly advantageous in densely packed resonator arrays. It additionally enables efficient free-space detection without deteriorating the cavity's quality factor. This is especially desirable for applications such as biosensing, which require spectral analysis with high signal-to-noise ratios to track resonance peaks. Implementing the micromirror concept into lab-on-chip systems may offer additional advantages: Sealing the micromirror with a transparent lid will create a defined volume surrounding the cavity, serving as a fluidic chamber. The analyte may be applied to the chamber through openings in the lid. The presented read-out concept may be applied to read-out multiple resonators or even coupled resonators [21] placed inside the micromirror.

Acknowledgments

The authors gratefully acknowledge technical support from Marko Heiler, Marc Schneider (both IMT, KIT), and Laszlo Leithold. We thank Naresh Kotadiya for the CAD drawing and Fabian Ruf (APH, KIT) and Dr. Sven Burger (Zuse Institute Berlin) for fruitful discussions on the FEM simulations. We further acknowledge JCMwave GmbH for academic use of their JCMsuite. T. W. and S. K. acknowledge financial support from the Karlsruhe School of Optics and Photonics (KSOP). T. M.'s Young Investigator Group YIG 08 received financial support from the 'Concept for the Future' of Karlsruhe Institute of Technology within the framework of the German Excellence Initiative. This work was partly carried out with the support of the Karlsruhe Nano Micro Facility (KNMF, www.knmf.kit.edu), a Helmholtz Research Infrastructure at Karlsruhe Institute of Technology (KIT, www.kit.edu), and with the support of the Alfried Krupp von Bohlen und Halbach Foundation. We acknowledge support by Deutsche Forschungsgemeinschaft and Open Access Publishing Fund of Karlsruhe Institute of Technology.

#225019 - $15.00 USD Received 16 Oct 2014; revised 6 Dec 2014; accepted 8 Dec 2014; published 16 Jan 2015